Friction **8**(2): 311–322 (2020)
https://doi.org/10.1007/s40544-018-0256-0
ISSN 2223-7690
CN 10-1237/TH

RESEARCH ARTICLE

Variation of the friction conditions in cold ring compression tests of medium carbon steel

Dawei ZHANG[1,2,*], **Bingkun LIU**[1], **Jingxiang LI**[1], **Minchao CUI**[1], **Shengdun ZHAO**[1]

[1] *School of Mechanical Engineering, Xi'an Jiaotong University, Xi'an 710049, China*

[2] *Key Laboratory of High Performance Complex Manufacturing, Central South University, Changsha 410083, China*

Received: 27 May 2018 / Revised: 19 October 2018 / Accepted: 06 November 2018

Abstract: Lubrication and friction conditions vary with deformation during metal forming processes. Significant macro-variations can be observed when a threshold of deformation is reached. This study shows that during the cold compression processing of #45 (AISI 1045) steel rings, the magnitude of friction and surface roughness (R_a) changes significantly upon reaching a 45% reduction in ring height. For example, the R_a of compressed ring specimens increased by approximately 55% immediately before and after reaching this threshold, compared to an 18% or 25%variation over a 35%–45% or a 45%–55% reduction in height, respectively. The ring compression test conducted by this study indicates that the Coulomb friction coefficient μ and Tresca friction factor m are 0.105 and 0.22, respectively, when the reduction in height is less than 45%; and 0.11 and 0.24, respectively, when the reduction in height is greater than 45%.

Keywords: friction condition; ring compression test; friction calibration curve; surface topography

1 Introduction

Friction has a significant influence on metal forming processes. Classic models, such as the Coulomb (Eq. (1)) and Tresca (or constant shear friction) (Eq. (2)) friction models are often used to describe the friction that occurs at a die-workpiece interface:

$$\tau = \mu p \tag{1}$$

$$\tau = mK \tag{2}$$

where τ is the frictional shear stress; μ is the Coulomb friction coefficient; p is the normal pressure; m is the Tresca friction factor; and K is the yield stress in shear.

The Coulomb friction coefficient and Tresca friction factor are key boundary conditions for the analysis of metal forming processes. Thus, it is necessary to determine their magnitude under specific lubrication conditions. However, these magnitudes are difficult to measure when forming bulk metal due to factors such as the complex tribological behaviors caused by severe plastic deformation, large mechanical loads, and various die surface treatments [1–5]. As such, friction tests, such as ring compression [6, 7], double cup extrusion [8, 9], T-shape compression [10], and barrel compression [11] tests have been developed to simulate the friction conditions that occur during metal forming processes.

The ring compression test is a proven approach for determining μ or m for bulk forming process. It is a simple, rapid, indirect, and inexpensive approach using standard rings and flat dies [12]. All that is necessary for friction conditions to be determined is measurement of the inner diameter of ring. Thus, it has been widely applied to the analysis of friction for bulk metal forming processes [7, 13]. Several variations of ring compression tests have been developed for specific operating conditions. For example, concave-ring and convex-ring tests have been developed for the analysis of friction

* Corresponding author: Dawei ZHANG, E-mail: zhangdawei2000@mail.xjtu.edu.cn

conditions at 'low' and 'high' pressures, respectively [14, 15]. Furthermore, an incremental ring test [16] has been developed to simulate re-loading and re-lubricating procedures for spline or thread rolling processes [17–19].

To determine the magnitude of μ or m, experimental data from the measurement of changes to the inner diameter of compressed rings are compared with friction calibration curves. This provides estimates of their value under various friction conditions. Commonly, calibration curves for ring compression tests predict changes to the inner diameter based on a reduction in height. Friction calibration curves are elaborated either by using analytical methods or the finite element method (FEM).

Pioneering experimental work by Male and Cockcroft [6] to determine these curves in the 1960s was followed by the implementation of several theoretical approaches, such as the slab method [20, 21] and the upper-bound method [22] to elaborate friction calibration curves for ring compression tests. However, these curves did not consider the influence of material and compression conditions on metal forming processes. Later, Sofuoglu and Rasty [23] used FEM to elaborate friction calibration curves for ring compression tests on black and white plasticines to enable these variables to be analyzed. Since this time, FEM has been widely used to elaborate friction calibration curves for ring compression tests [24]. It has also been used to elaborate curves for double cup extrusion [9], T-shape compression [10], and barrel compression tests [25, 26].

Male [27] also found that while a variation in friction coefficients during ring compression tests under dry conditions for aluminum, titanium, mild steel, and alpha-brass was significant, it remained constant for alpha-brass ring specimens under lubricated conditions. Disc-compression tests conducted in the Ref. [27] also confirmed this result. This means that in general, friction coefficient or factor used in finite element analysis (FEA) for bulk metal forming processes can be assumed to be constant. Thus the magnitude of friction can also be regarded as constant for friction tests under lubricated conditions.

However, variable friction models have also been developed, such as Wanheim-Bay's general friction model (Eq. (3)) [28, 29]:

$$\tau = f\alpha K \tag{3}$$

where f is the friction factor; and α is the ratio of real to apparent contact area. Generally, these models use a variable expression for α to describe friction conditions. In this instance, f is evaluated analytically using an approach such as the slip-line field method [30] or by comparing experimental results with friction calibration curves [31]. The ratio of real to apparent contact area is then determined analytically using several complex analytical expressions [29, 30].

The f in Wanheim-Bay's model is similar to the m in the Tresca model, and in some studies f in Eq. (3) has been written as m [30]. The corresponding values for f and m evaluated by ring compression tests are different, however, the shape of the resulting friction calibration curves are similar [29]. In barrel compression tests, the shapes of curves for the friction area ratio under corresponding results for f and m are also similar [32]. However, the implementation of the FEM code has some limitations for complex processes. For example, it was not implemented for some 3D commercial codes for bulk forming processes, such as DEFORM. Coulomb and Tresca friction models are often adopted by commercial codes for FEA of bulk forming processes due to their simplicity and numerical rigidity [32, 33]. Wanheim-Bay's friction model is much better applied at the micro-scale for applications such as micro forming [34] and powder compaction [35] processes. Thus, the discussion in this study focuses on the Coulomb and Tresca friction models.

Often experimental data from cold ring compression tests for medium carbon steel under lubricated conditions cannot be fitted to a single calibration curve, while achieving an error below 0.5%. In this case, the discrepancy between experimental data and calibration curves will be high for some data points. Thus, a variable magnitude of friction determined by ring compression tests for the cold forming of medium carbon steel (AISI 1045) was investigated in this study. Friction calibration curves were elaborated using the FEM to consider material properties. The results indicate that predicting friction conditions accurately requires two calibration curves to describe the experimental data at former and latter compression stages, respectively. The value for surface roughness R_a was found to increase in proportion to the reduction in the height of the ring. However, this relationship

changed sharply once a threshold of a 45% reduction in height was reached. At this point, R_a increased by more than 50% over a 1% reduction in height. The magnitude of friction was also observed to change significantly immediately before and after this threshold.

2 Ring compression test

2.1 Ring specimens

A standard ring with a rectangular cross-section was used for the compression test made from #45 Chinese grade steel, which is equivalent to U.S. standard AISI 1045. Its chemical composition is listed in Table 1 based on the Chinese standard. The relationship between the stress and strain of #45 steel acquired by uniaxial tension is shown in (Eq. (4)) [16].

$$\sigma = 1450\left(0.0132715+\varepsilon\right)^{0.2817} \tag{4}$$

where σ is the stress; ε is the plastic strain.

Standard relative ring dimensions ($D_0 : d_0 : h_0 = 6:3:2$) were adopted for this experiment, where D_0, d_0, and h_0 are the initial outer diameter, inner diameter and height of ring specimen, respectively. The values of these variables were 21, 10.5, and 7 mm, as shown in Fig. 1. The upper and lower surfaces of ring specimen were machined by a turning process to a surface roughness (R_a) of approximately 3.2 μm.

2.2 Experimental equipment

The predicted forming load for a 60% reduction in height of the ring specimen described in Section 2.1 is larger than 140 tons, as shown in Fig. 2. Thus, a 160-ton screw press (J53-160B, Qingdao Forging Machinery Factory, China) was used to conduct the ring compression experiment.

Table 1 Chemical composition of #45 steel.

	C	Si	Mn	P	S	Cr	Ni	Cu
wt%	0.42–0.50	0.17–0.37	0.50–0.80	≤0.035	≤0.035	≤0.25	≤0.30	≤0.25

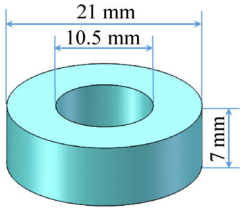

Fig. 1 Dimensions of the ring specimen.

Based on the dimensions of ring specimen and the structure of screw press, the dies shown in Fig. 3(a) were designed and manufactured as shown in Fig. 3(b). The platens of the upper and lower die shown in Fig. 3 were made from T8 die steel (ASTM Grade: W1A-8), while the other components were made from carbon steel.

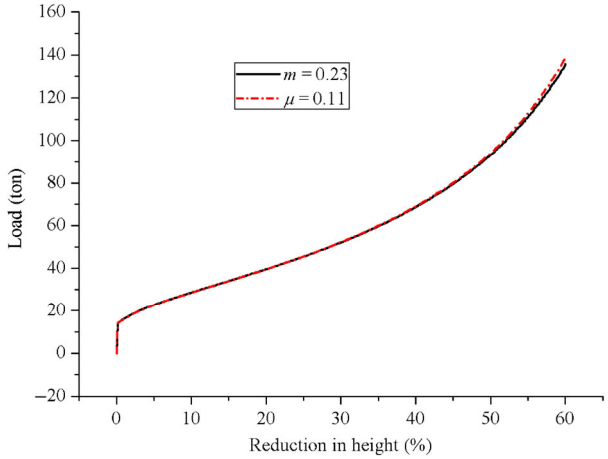

Fig. 2 Predicted load during ring compression process by FEM.

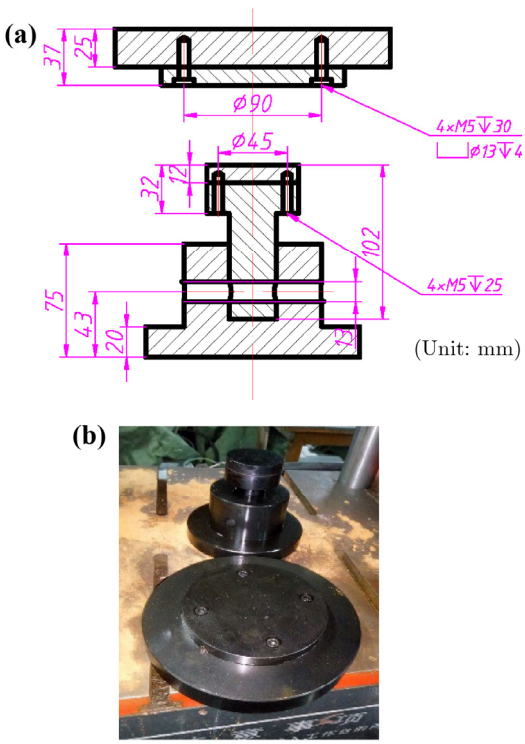

Fig. 3 Combined die for the ring compression experiments: (a) dimensions of the die, (b) photo of the die set.

2.3 Implementation of the ring compression test

The screw press is a forging apparatus. The metal forming created by the screw press is implemented by a combination of the kinetic energy (E) produced by the working mechanisms of screw press including the flywheel, screw, and slider, as well as the stored energy (E) in the working mechanisms expressed as follows [36]:

$$E = \frac{1}{2}mv^2 + \frac{1}{2}J\omega^2 \tag{5}$$

where m is the weight (kg) of flywheel, screw, and slider; J is the moment of inertia (kg·m^2) of the flywheel and screw; v is the maximum speed (m/s) of the slider when the press blows; and ω is the maximum angular velocity (rad/s) of the flywheel when the press blows.

The moving parts (the flywheel, screw, and slider) are gradually accelerated and the kinetic energy of these parts is increased until the upper die contacts the billet and they stop rapidly. The billet absorbs the energy and yields (plastic deformation). The blow energy E consists of both linear and rotary motion energy. The reduction in the height of the metal ring can be controlled by adjusting the blow energy, which affects the amount of stored energy that is released. During the ring compression process by the screw press, a small reduction in height can be controlled by adjusting the gravity energy of slider. A large reduction in height can be achieved by adjusting the speed of the flywheel. The motion is adjusted by controlling the accelerating time and the stroke.

Prior to the compression tests, the ring specimens were cleaned and lubricated with hydraulic oil (HM-46). The minimum inner diameters and the reduction in height of rings after compression were measured using vernier calipers. The inner diameter was measured at 120° intervals along the circumference and an average value was used to calculate the percentage change to the inner diameter. The height and percentage reduction in height was also measured and calculated by this way.

Confidence intervals for the mean and standard deviation were used to evaluate the reliability of the experimental data. Equation 6 [37] was used to calculate confidence intervals for the mean diameter, where a significance level of 0.05 to obtain a 95% confidence interval.

$$\bar{x} \pm \frac{\sigma}{\sqrt{n}} K_{\frac{\alpha}{2}} \tag{6}$$

where $\bar{x}$ is the mean; σ is the standard deviation; n is the sample number; $K_{\frac{\alpha}{2}}$ is the confidence limit; and α is the significance level.

A total of sixteen compression tests were conducted and the resulting shapes of the compressed ring specimens after different reductions in height are shown in Fig. 4.

3 Friction calibration curves based on the FEM

3.1 FE model of the ring compression process

An axisymmetric finite element (FE) model of the ring compression process was developed using commercial software called DEFORM. The model was verified and used for both cold ring compression test [16] and hot ring compression test [24]. It was then verified by comparing the results with the applied load. Thus, the numerical results obtained in the present study can be deemed valid.

The #45 steel used in the experiment is a strain hardening material under cold forming conditions [16]. The data for AISI 1045 steel from the DEFORM material database at room temperature indicates that the stress-strain curve for a strain rate of 1.5 is almost the same as the stress-strain curve for a strain rate of 100. This indicates that #45 (AISI 1045) steel is a rate-independent material for cold forming processes. A temperature-independent material model is often used for cold forming conditions [31–33]. Thus, only strain hardening materials were considered for modeling by this study, enabling Eq. (4) to be used.

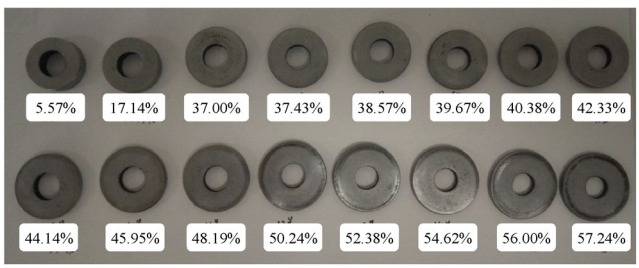

Fig. 4 Compressed ring specimens.

A quadrilateral element was used for the initial meshing and re-meshing of the FE model. For the initial meshes, 8130 elements were used, and the minimum mesh size was less than 0.03 mm. The von Mises yield criterion was adopted within the FE model. Coulomb and Tresca friction models were used to describe the friction at the interface between ring and the die, respectively.

3.2 Elaborated friction calibration curves by numerical results

Friction calibration curves for the ring compression tests are elaborated by either analytical methods or the FEM. Curves elaborated by the FEM are more accurate than those elaborated by analytical methods [23, 24], as the material properties and forming conditions can be considered. Thus, the FEM was used to elaborate friction calibration curves for this study. These curves only have numerical dependency.

The height (h) and inner diameter (d) of metal ring during the compression process could then be predicted with numerical simulations. Then, a reduction percentage for both the height (δh) and inner diameter (δd) could be calculated using the following equations:

$$\delta h = \frac{h_0 - h}{h_0} \times 100\% \tag{7}$$

$$\delta d = \frac{d_0 - d}{d_0} \times 100\% \tag{8}$$

According to the numerical results, the friction calibration curves for both the Coulomb and Tresca friction models could be elaborated, where the minimum inner diameters from the FEM are used. A loading speed of v = 1 mm/s was adopted for the FEA to generate calibration curves. The height and inner diameter of ring obtained from the experiment in Section 2.3 was calculated by Eqs. (7) and (8). Figure 5 illustrates the friction calibration curves and experimental results, where the curves were generated through FEA, while dots were obtained experimentally.

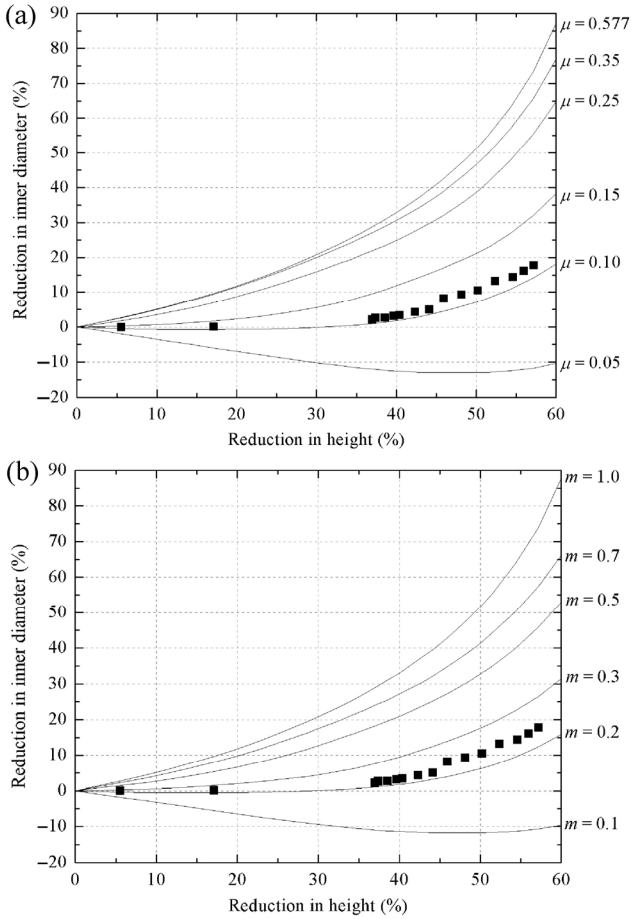

Fig. 5 Friction calibration curves and experimental data (curves are generated with FEA while dots are obtained experimentally): (a) with the μ calibration curves and (b) with the m calibration curves.

4 Discussion

4.1 Friction conditions

The Coulomb friction coefficient and Tresca friction factor were determined by comparing experimental results with the friction calibration curves, as shown in Fig. 5. However, there is no clear standard for determining how to match the experimental results with the most appropriate calibration curve, which is the key to evaluating friction conditions.

To determine the relationship between Coulomb friction coefficient and Tresca friction factor, Eq. (9) was defined as a standard [38]. If the inner diameters of the ring specimens at a 50% reduction in height correspond with Eq. (9), then the value for μ is deemed to be a match with the value for m.

$$\frac{\left|d_\mu - d_m\right|}{d_0} < e \tag{9}$$

where d_μ is the inner diameter of metal ring under the Coulomb's friction model; d_m is the inner diameter of

ring specimen under the Tresca friction model; d_0 is the initial inner diameter of ring specimen, and e is a smaller positive number.

The FEM results in the study [38] indicate that when $e < 0.005$, the inner diameter remains the same with only a slight variation in friction condition due to accuracy of FE model. Thus, $e = 0.005$ is a suitable value for determining whether the reduction in the inner diameter of the metal ring matches with the correct calibration curve. Based on Eq. (9), Eq. (10) was defined to evaluate the friction conditions and $e = 0.005$ or 0.5% was adopted as the small positive number.

$$\frac{\left|d_{\mathrm{Exp}} - d_{\mu,m}\right|}{d_0} = \left|\delta d_{\mathrm{Exp}} - \delta d_{\mu,m}\right| < e \tag{10}$$

where d_{Exp} and δd_{Exp} are the inner diameter and reduction percentage for the inner diameter, respectively. With a small change in μ or m, changes to the inner diameter are insignificant for a small reduction in height; however, they are significant after a 30% reduction in height. Using Eq. (10), the differences between the experimental results and appropriate calibration curves were calculated and listed in Table 2. It was found that the experimental data were difficult to fit to only one calibration curve accurately and several errors were greater than 0.5%. For example, when the reduction in height of the ring specimen was less than 45%, the difference between the experimental data and FEM data for $\mu = 0.11$ or $m = 0.24$ was much higher than the results for $\mu = 0.105$ or $m = 0.22$. However, the opposite was true, when the reduction in height was greater than 45%.

Table 2 Differences between the experimental results and the calibration curve.

δh (%)	$\left\|\delta d_{\mathrm{Exp}} - \delta d_{\mu,m}\right\|$ (%)					
	μ = 0.105	μ = 0.1075	μ = 0.11	m = 0.22	m = 0.23	m = 0.24
37.00	0.350	0.483	1.934	0.240	0.537	1.845
37.43	0.240	0.627	1.662	0.169	0.468	1.553
38.57	0.325	0.734	1.783	0.056	0.603	1.672
39.67	0.195	0.606	1.982	0.058	0.519	1.883
40.38	0.236	0.783	2.042	0.061	0.638	1.948
42.33	0.103	0.873	1.893	0.140	0.762	2.010
44.14	0.073	0.921	1.873	0.337	0.932	1.927
45.95	2.552	1.054	0.489	2.361	1.163	0.458
48.19	2.024	1.135	0.163	2.135	1.046	0.032
50.24	1.967	0.844	0.089	2.077	0.934	0.396
52.38	2.225	0.972	0.572	2.236	0.982	0.305
54.62	1.864	0.452	0.109	1.973	0.723	0.389
56.00	1.776	0.692	0.216	1.867	0.697	0.105
57.24	1.953	0.788	0.406	1.962	0.779	0.125

Thus, different friction conditions should be used to describe the experimental data both before and after the threshold reduction in height. When 35% < δh < 45%, the experimental data is best fitted to a calibration curve with $m = 0.22$ or $\mu = 0.105$. Alternatively when δh > 45%, the experimental data is best fit to a calibration curve with $m = 0.24$ or $\mu = 0.11$. This is shown in Fig. 6, where the experimental data is plotted with confidence intervals, presented as error bars. The short confidence intervals for most of the experimental

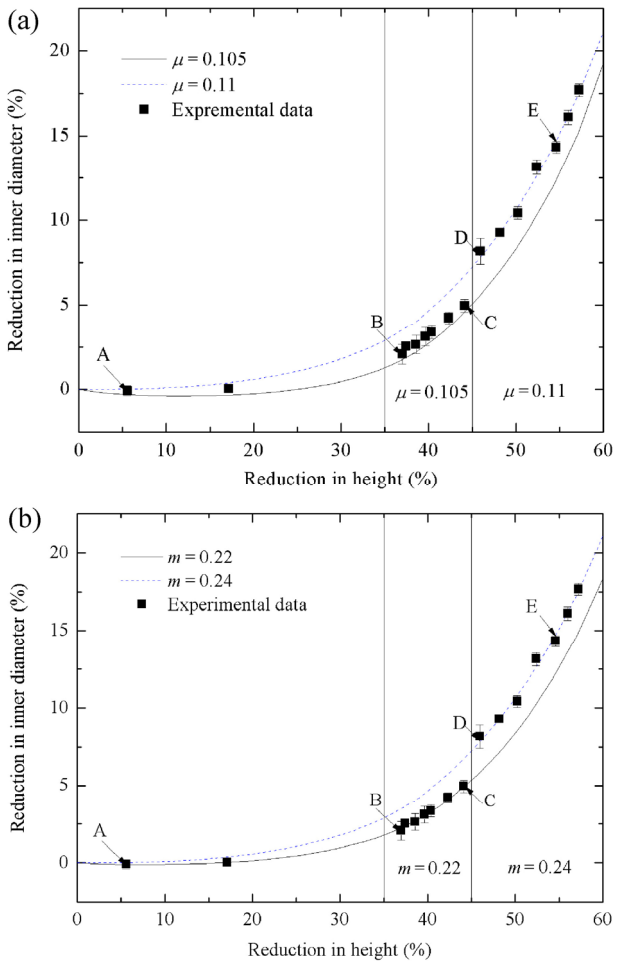

Fig. 6 Experimental data and matching calibration curve: (a) with the μ calibration curves and (b) with the m calibration curves.

data indicate that the average measured inner diameter is precise. This also demonstrates that the ring compression tests produced accurate results, with no abnormal data. The friction conditions change sharply at a 45% reduction in height. This finding is similar to results obtained for the compression of aluminum discs under dry friction [27], where conditions changed significantly at a 37% reduction in height.

4.2 Surface topography

Friction conditions during the ring compression process changed significantly when a 45% reduction in height for the ring specimens was reached and could be divided into two specific stages. A laser confocal microscope (OLS4000, Olympus®) was used to investigate changes to the surface topography of the compressed metal rings at a resolution of 0.12 μm as these conditions changed.

According to the analysis in Section 4.1, five compressed ring specimens (A, B, C, D, and E) were selected for measurement, as shown in Fig. 6. The reduction in height of the chosen metal ring samples was 5.57%, 37.43%, 44.14%, 45.95%, and 54.62%, respectively, and the corresponding shapes are shown in Fig. 4. Considering the data listed in Table 2, these five ring specimens, particularly specimens B, C, D, and E, were chosen to evaluate the continuity of the curves described by the experimental data in Fig. 6. To observe the topographical characteristic along the radial direction, two surface zones were observed from the inside and outside of upper surface of the compressed ring specimen, respectively. The inner zone was approximately 0.5 mm from the inside edge of surface, and the outer zone was approximately 0.5 mm from outside edge of the surface. The area of the observed zones was 256 μm × 256 μm. Figure 7 illustrates the surface topography from each of these five ring specimens.

Surface fluctuations were found to be larger in the outer zones than in the inner zones and increased as the height of the rings decreased. The changes in surface fluctuation that occurred within 1% of a 45% reduction in height were significantly greater than the changes observed between a 35%–45% and 45%–55% reduction in height. Similar changes were observed for the results obtained for surface roughness (R_a).

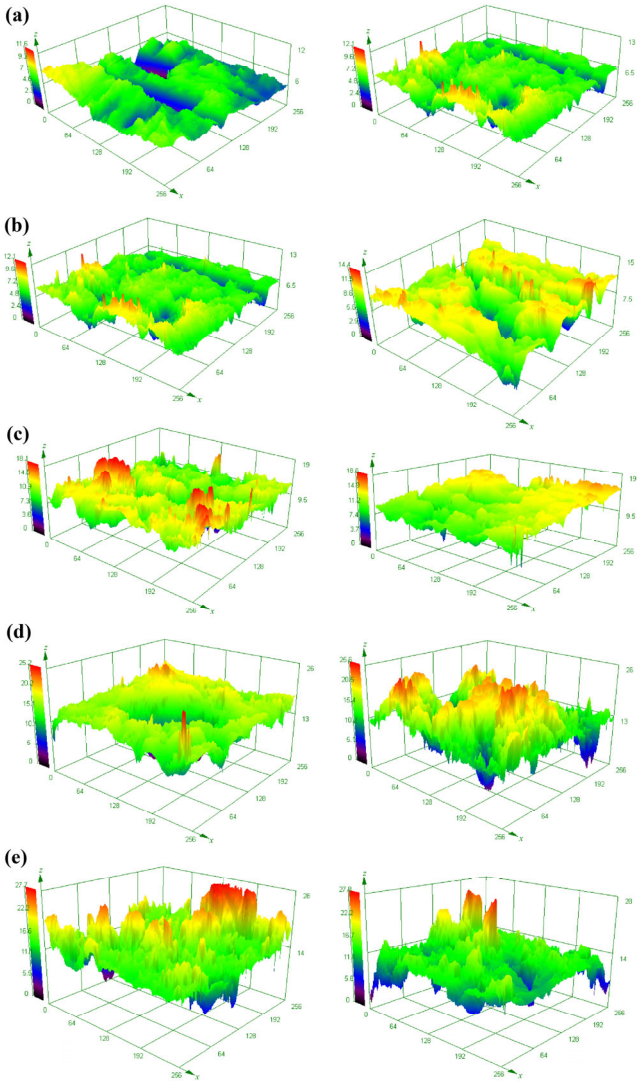

Fig. 7 Surface topography of the compressed ring specimens (Unit: μm), with a reduction in height of: (a) 5.57% (compressed ring A), (b) 37.43% (compressed ring B), (c) 44.14% (compressed ring C), (d) 45.95% (compressed ring D), and (e) 54.62% (compressed ring E). For each set of images, the first image is for the inner observation zone and the second is for the outer observation zone.

Figure 8 illustrates the changes to surface roughness of the ring specimens during the compression tests.

Five sampling lines from the observed 256 μm × 256 μm zones were used to measure surface roughness, as shown in Fig. 9. The surface roughness (R_a) was calculated for one sampling line. Then, five values of surface roughness could be obtained for each observed zone, before Eq. (6) was used to calculate the value. To obtain accurate results, the sampling lines needed to be perpendicular to the region experiencing large

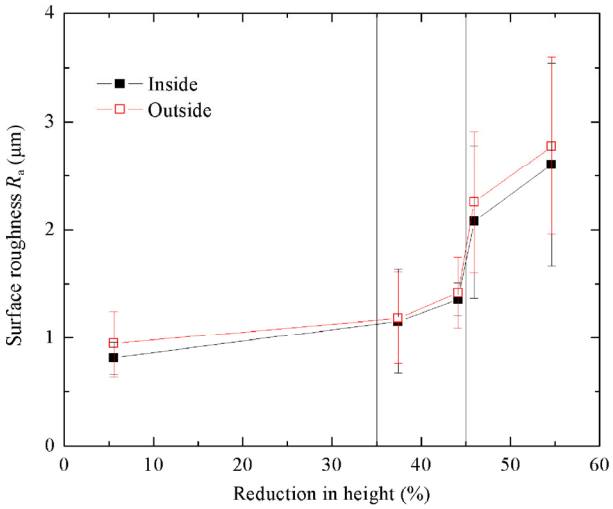

Fig. 8 Surface roughness of the compressed ring specimens.

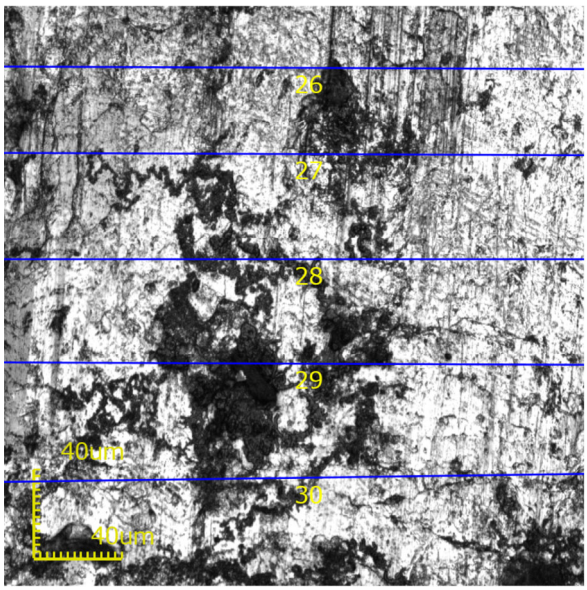

Fig. 9 Sketch of sampling line in the observed zone.

surface fluctuations and the five sampling lines needed to be distributed as evenly as possible within the observed zone. Figure 7 shows that the surface fluctuations in the observed zone are distributed irregularly along the x or y-axis. This means that there are large fluctuations along each sampling line. Thus, compared to Fig. 6, wide confidence intervals can be observed for the results shown in Fig. 8, despite using more measuring times.

It was found that the values for surface roughness in the outer zone of each of the five samples were greater than measured for the inner zone. However, the difference in R_a between inner and outer zones was smaller. The value for R_a varied notably with an increasing reduction in height of the ring specimen. The surface roughness (R_a) of the inner and outer zones increased by 18% and 20%, respectively, over a reduction in height from 35% to 45%; and increased by 25% and 23%, respectively, over a reduction in height from 45% to 55%. However, the value for R_a changed dramatically around a 45% reduction in height, where the Coulomb friction coefficient (μ) and Tresca friction factor (m) also changed. The R_a for the inner and outer zones increases by approximately 53% and 59%, respectively, from a 44.14% to a 45.95% reduction in height.

The interaction between surface roughness and friction conditions has previously been proven in Ref. [39]. With an increase in the reduction of height, the weight of liquid lubricant reduces as it is squeezed away from the interface [16, 40]. In this case, lubrication is less effective, while there is an increase in surface roughness. The interface area between die and ring is enlarged and this further reduces the effectiveness of lubrication. As the surface fluctuations increase, the increase in the outer interface area is larger than the inner interface area. This may be one reason why surface roughness in the outer zone is larger than the inner zone. Additionally, pressure at interface also plays an important role in changing surface roughness. Figure 10 illustrates the changes to the contact stress (δ_z) (z-axis is the compressed direction) at the interface between the ring and die. The δ_z is shown to increase with a reduction in the height of ring specimen and an increasing magnitude of friction. The δ_z at the inner and outer edge is an extremum, which means that the change closest to the edge of each region of the interface is most significant. Comparatively, the change in the middle region of the interface between inner and outer zones is gentle. However, the δ_z distributed along radial direction in the middle region also fluctuates significantly at a large reduction in height, particularly after a 45% reduction in height occurs as shown in Fig. 10. High contact stress combined with less effective lubrication increases the surface roughness. The δ_z for the inner region is less than for that of the outer region. This may be another reason why the outer surface is rougher than the inner surface.

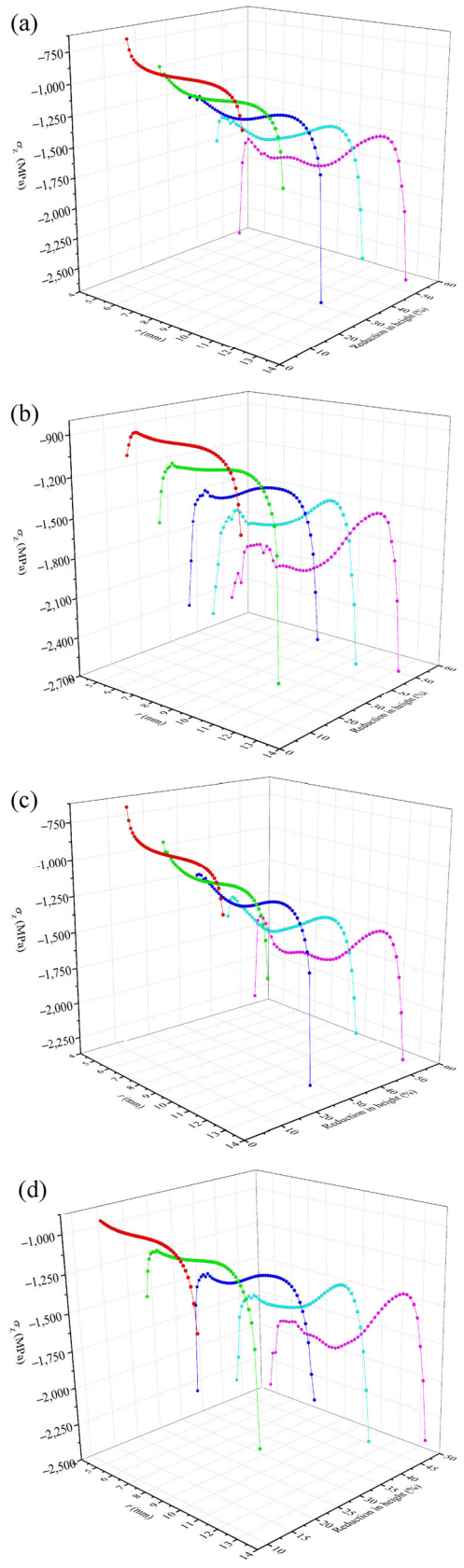

Fig. 10 Contact stress at the interface predicted by the FEM: (a) $\mu = 0.1$, (b) $\mu = 0.15$, (c) $m = 0.2$, and (d) $m = 0.3$.

With an increasing reduction in the height of the ring specimen, the lubricant present at the interface is reduced and the interface area enlarges. In this case, the surface topography is changed by the deformation of the metal and the surface roughness increases. Under a small deformation, such as a 5.57% reduction in height, the observed surface topography is flat, as shown in Fig. 7(a). The surface roughness (R_a) is also small, as shown in Fig. 8. These results support the above-mentioned conclusions. When less effective lubrication combined with increased stress reaches a threshold, the magnitude of friction changes. The threshold in cold ring compression tests of #45 (AISI 1045) steel is a 45% reduction in height according to the results of this study. However, the material properties and friction conditions (such as a dry condition, or with lubrication by different materials) have a significant impact on this threshold. For example, the friction coefficient changes under dry conditions but remains constant when lubricated in the study [27].

5 Conclusions

In this study, a cold ring compression test was conducted on medium carbon steel and the friction conditions were evaluated to a low error (0.5%). Then, the compressed ring specimens for specific height reductions were selected according to variations in friction conditions and their surface topography was measured. The following conclusions were drawn:

(1) During the compression process of the ring specimen, the surface topography changed and the value for surface roughness increased. The surface topography and surface roughness underwent a significant change of more than 50% at a height reduction of 45%. A difference in the surface topography or surface roughness between the inner and outer surface of the compressed ring specimen was observed, however, this difference was found to be negligible.

(2) The surface roughness (R_a) of the compressed ring specimen increased by approximately 20% and 25% between a 35% and 45% and a 45% and 55% reduction in height, respectively. However, the surface roughness (R_a) of the compressed ring specimen increased by approximately 55% over a 1% variation from a 45% reduction in height.

(3) Experimental data are difficult to fit to a single calibration curve accurately. To fit the data within the specified error of 0.5% using Eq. (11), a Coulomb friction coefficient (μ) of 0.105 was determined when $\delta h < 45\%$ and 0.11 was determined when $\delta h > 45\%$. A Tresca friction factor (m) of 0.22 was determined when $\delta h < 45\%$ and 0.24 was determined when $\delta h > 45\%$.

Acknowledgements

The authors would like to gratefully acknowledge the support of the National Natural Science Foundation of China (Grant Nos. 51675415 and 51335009) and the Open Research Fund of the Key Laboratory of High-Performance Complex Manufacturing, Central South University (Kfkt2016-06).

References

[1] Kalpakjian S. Recent progress in metal forming tribology. *CIRP Ann* **34**(2): 585–592 (1985)

[2] Dohda K, Boher C, Rezai-Aria F, Mahayotsanun N. Tribology in metal forming at elevated temperatures. *Friction* **3**(1): 1–27 (2015)

[3] Zhang D W, Yang H. Numerical study of the friction effects on the metal flow under local loading way. *Int J Adv Manuf Technol* **68**(5–8): 1339–1350 (2013)

[4] Wang D, Yang H, Li H. Advance and trend of friction study in plastic forming. *Trans Nonferrous Met Soc China* **24**(5): 1263–1273 (2014)

[5] Katoch S, Sehgal R, Singh V. Optimization of friction and wear characteristics of varied cryogenically treated hot die steel grade AISI-H13 under dry condition. *Friction* **5**(1): 66–86 (2017)

[6] Male A T, Cockcroft M G. A method for the determination of the coefficient of friction of metals under conditions of bulk plastic deformation. *J Inst Metals* **93**(2): 38–46 (1964)

[7] Altan T, Oh S I, Gegel H L. *Metal Forming: Fundamentals and Application*. Metal Park (USA): American Society for Metals, 1983.

[8] Buschhausen A, Weinmann K, Lee Y L, Altan T. Evaluation of lubrication and friction in cold forging using a double backward-extrusion process. *J Mater Process Technol* **33**(1–2): 95–108 (1992)

[9] Gariety M, Ngaile G, Altan T. Evaluation of new cold forging lubricants without zinc phosphate precoat. *Int. J Mach Tool Manuf* **47**(3–4): 673–681 (2007)

[10] Zhang Q, Felder E, Bruschi S. Evaluation of friction condition in cold forging by using T-shape compression test. *J Mater Process Technol* **209**(17): 5720–5729 (2009)

[11] Ebrahimi R, Najafizadeh A. A new method for evaluation of friction in bulk metal forming. *J Mater Process Technol* **152**(2): 136–143 (2004)

[12] Groche P, Müller C, Stahlmann J, Zang S. Mechanical conditions in bulk metal forming tribometers—Part one. *Tribol Int* **62**: 223–231 (2013)

[13] Lange K. *Handbook of Metal Forming*. New York (USA): McGraw-Hill, 1985.

[14] Petersen S B, Martins P A F, Bay N. An alternative ring-test geometry for the evaluation of friction under low normal pressure. *J Mater Process Technol* **79**(1–3): 14–24 (1998)

[15] Tan T, Martins P A F, Bay N, Zhang W. Friction studies at different normal pressures with alternative ring-compression tests. *J Mater Process Technol* **80–81**: 292–297 (1998)

[16] Zhang D W, Cui M C, Cao M, Ben N Y, Zhao S D. Determination of friction conditions in cold-rolling process of shaft part by using incremental ring compression test. *Int J Adv Manuf Technol* **91**(9–12): 3823–3831 (2017)

[17] Zhang D W, Li Y T, Fu J H, Zheng Q G. Rolling force and rolling moment in spline cold rolling using slip-line field method. *Chin J Mech Eng* **22**(5): 688–695 (2009)

[18] Zhang D W, Zhao S D, Ou H A. Analysis of motion between rolling die and workpiece in thread rolling process with round dies. *Mech Mach Theory* **105**: 471–494 (2016)

[19] Zhang D W. Die structure and its trial manufacture for thread and spline synchronous rolling process. *Int J Adv Manuf Technol* **96**(1–4): 319–325 (2018)

[20] Burgdorf M. Über die Ermittlung des Reibwertes für Verfahren der Massivum formung Durch den Rings tauchversuch. *Industrie-Anzeiger*, **89**(39): 15–20 (1967)

[21] Hawkyard J B, Johnson W. An analysis of the changes in geometry of a short hollow cylinder during axial compression. *Int J Mech Sci* **9**(4): 163–182 (1967)

[22] Lee C H, Altan T. Influence of flow stress and friction upon metal flow in upset forging of rings and cylinders. *J Eng Ind* **94**(3): 775–782 (1972)

[23] Sofuoglu H, Rasty J. On the measurement of friction coefficient utilizing the ring compression test. *Tribol Int* **32**(6): 327–335 (1999)

[24] Zhang D W, Yang H, Li H W, Fan X G. Friction factor evaluation by FEM and experiment for TA15 titanium alloy in isothermal forming process. *Int J Adv Manuf Technol* **60**(5–8): 527–536 (2012)

[25] Yao Z H, Mei D Q, Shen H, Chen Z C. A friction evaluation method based on barrel compression test. *Tribol Lett* **51**(3): 525–535 (2013)

[26] Fan X G, Dong Y D, Yang H, Gao P F, Zhan M. Friction assessment in uniaxial compression test: A new evaluation method based on local bulge profile. *J Mater Process Technol* **243**: 282–290 (2017)

[27] Male A T. Variations in friction coefficients of metals during compressive deformation. *J Inst Metals* **94**(4): 121–125 (1966)

[28] Wanheim T. Friction at high normal pressures. *Wear* **25**(2): 255–244 (1973)

[29] Petersen S B, Martins P A F, Bay N. Friction in bulk metal forming: A general friction model vs. the law of constant friction. *J Mater Process Technol* **66**(1–3): 186–194 (1997)

[30] Wanheim T, Bay N. A model for friction in metal forming processes. *CIRP Ann* **27**(1): 189–194 (1978)

[31] Fereshteh-Saniee F, Pillinger I, Hartley P. Friction modelling for the physical simulation of the bulk metal forming processes. *J Mater Process Technol* **153–154**: 151–156 (2004)

[32] Tan X C. Comparisons of friction models in bulk metal forming. *Tribol Int* **35**(6): 385–393 (2002)

[33] Joun M S, Moon H G, Choi I S, Lee M C, Jun B Y. Effects of friction laws on metal forming processes. *Tribol Int* **42**(2): 311–319 (2009)

[34] Wang C J, Guo B, Shan D B, Zhang M M, Bai X M. Tribological behaviors in microforming considering microscopically trapped lubricant at contact interface. *Int J Adv Manuf Technol* **71**(9–12): 2083–2090 (2014)

[35] Güner F, Sofuoglu H, Cora Ö N. An investigation of contact interactions in powder compaction process through variable friction models. *Tribol Int* **96**: 1–10 (2016)

[36] Wang M, Fang L, Zhao S D, Wen S P. *Equipment and Their Automation of Material Forming*. Beijing (China): Higher Education Press, 2010.

[37] Compile Group for Handbook of Mathematics. *Handbook of Mathematics*. Beijing: Higher Education Press, 1979.

[38] Zhang D W, Ou H A. Relationship between friction parameters in a Coulomb-Tresca friction model for bulk metal forming. *Tribol Int* **95**: 13–18 (2016)

[39] Groche P, Stahlmann J, Hartel J, Köhler M. Hydrodynamic effects of macroscopic deterministic surface structures in cold forging processes. *Tribol Int* **42**(8): 1173–1179 (2009)

[40] Li L X, Peng D S, Liu J A, Liu Z Q, Jiang Y. An experimental study of the lubrication behavior of A5 glass lubricant by means of the ring compression test. *J Mater Process Technol* **102**(1–3): 138–142 (2000)

Dawei ZHANG. He received his Ph.D. degree in materials processing engineering in 2012 from Northwestern Polytechnical University, Xi'an, China. After then, he joined School of Mechanical Engineering, Xi'an Jiaotong University. His current position is an associate professor at School of Mechanical Engineering. His research areas cover the plastic forming technology and equipment, hydraulic system, and friction in metal forming, etc.

Bingkun LIU. He received his bachelor degree in mechanical engineering in 2017 from Xi'an Jiaotong University, Xi'an, China. After that, he studied for a master's degree in mechanical engineering at the same university. His research interests include the plastic forming process and the friction conditions during the forming.

Jingxiang LI. He received his Ph.D. degrees in mechanical engineering from Xi'an Jiaotong University, China, and The University of Tokushima, Japan, in 2013 respectively. Then he joined School of Mechanical Engineering of Xi'an Jiaotong University, and as an associate professor from 2017. His research interests include electro-mechanical systems and plastic forming process.

Minchao CUI. He received his bachelor degree in vehicle engineering in 2009 from Xi'an Jiaotong University, Xi'an, China. After then, he was a double-degree program Ph.D. student in both of Xi'an Jiaotong University and Tokushima University, Tokushima, Japan. He has recently obtained two Ph.D. degrees at the above two universities. His research interests include intelligent structures and mechanics systems.

Shengdun ZHAO. He received his MS and Ph.D. degrees in mechanical engineering from School of Mechanical Engineering, Xi'an Jiaotong University, China, in 1986 and 1997, respectively. His current position is a professor at School of Mechanical Engineering, Xi'an Jiaotong University, China. His research areas cover the plastic forming technology and equipment, computer control of mechanical-electrical-hydraulic system, and fluid transmission and control, etc.